Control Characteristics of Magnetotactic Bacteria: *Magnetospirillum Magnetotacticum* Strain MS-1 and *Magnetospirillum Magneticum* Strain AMB-1

Islam S. M. Khalil[1] and Sarthak Misra[2]

[1]German University in Cairo, Cairo 13411, Egypt
[2]MIRA-Institute for Biomedical Technology and Technical Medicine, University of Twente, Enschede 7522, The Netherlands

Magnetotactic bacteria have the potential to execute nontrivial tasks, such as microactuation, micromanipulation, and microassembly, under the influence of the controlled magnetic fields. Closed-loop control characteristics of these magnetic microorganisms depend on their self-propulsion forces (motility) and magnetic dipole moments. These properties can be controlled through the growth conditions of magnetotactic bacteria. We provide a comparison between two species of magnetotactic bacteria, i.e., *Magnetospirillum magnetotacticum* strain MS-1 and *Magnetospirillum magneticum* strain AMB-1. This comparison includes the characterization of their morphologies, magnetic dipole moments, and closed-loop control characteristics in the transient and steady states. The characterized average magnetic dipole moments of motile cells of *M. magnetotacticum* and *M. magneticum* strains are 1.4×10^{-16} A.m^2 and 1.5×10^{-17} A.m^2 at a magnetic field of 7.9 mT, respectively. These magnetic dipole moments are used in the realization of closed-loop control systems for each bacterial strain. The closed-loop control systems achieve point-to-point positioning of *M. magnetotacticum* cells at an average velocity of 32 ± 10 μm/s (approximately seven body lengths per second), and within an average region of convergence of 23 ± 10 μm (approximately four body lengths), while cells of *M. magneticum* strain are positioned at an average velocity of 30 ± 12 μm/s (approximately eight body lengths per second), and within an average region of convergence of 35 ± 14 μm (approximately 14 body lengths). These results suggest that the cells of *M. magnetotacticum* strain have a slightly greater tendency to provide desirable closed-loop control characteristics than cells of *M. magneticum* strain.

Index Terms— **Characterization, control, *Magnetospirillummagneticum*, *Magnetospirillummagnetotacticum*, magnetotactic bacteria, microrobots.**

I. Introduction

CLOSED-LOOP control characteristics of the different strains of magnetotactic bacteria, which we refer to as biological microrobots, depend on the growth conditions [1], [2], which affect their morphologies, drag force and torque coefficients, magnetic dipole moments, and the self-propulsion forces generated by their flagella. Therefore, each strain of magnetotactic bacteria could show different transient- and steady-state closed-loop control characteristics. The dependency of the closed-loop control system on the aforementioned properties might allow one bacterial strain to provide desirable control characteristics than other strains. This might allow us to choose certain strain of magnetotactic bacteria during their utilization as biological microrobots.

Much efforts have been expended to characterize magnetotactic bacteria [1]–[7], while a few recent attempts have been done to control their motion [8]–[10]. Bahaj and James [11] presented offline motion analysis-based techniques to characterize the magnetic dipole moment of the magnetotactic bacteria. These techniques depend on the determination of the time and diameter of the U-turn trajectories of the motile magnetotactic bacterium (MTB) during reversals of the magnetic field. The magnetic dipole moment was also characterized by applying rotating magnetic fields, then the magnetic dipole moment was calculated using the boundary frequency after which a motile MTB can no longer follow the rotating fields [12], [13]. Magnetic dipole moment of nonmotile magnetotactic bacteria was characterized by measuring the flip time of an MTB during the reversal of the magnetic fields [14].

Characterization of *Magnetospirillum magnetotacticum* strain MS-1 was done using motile and nonmotile techniques [15]. The motile techniques depend on the determination of the U-turn time and diameter, and boundary frequency of the MTB, whereas the nonmotile technique depends on the morphology, flip time, and the number of

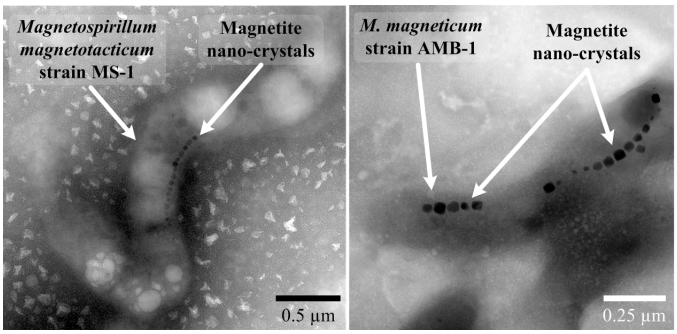

Fig. 1. TEM images of the MTB. The TEM images show the cells that envelope chains of magnetite nanocrystals. An MTB passively align itself along the magnetic field lines due to the exerted torque on its magnetic dipole. Left: *M. magnetotacticum* strain MS-1. Cell of the *M. magnetotacticum* strain has an average diameter and length of 0.5 ± 0.1 and 5.2 ± 0.5 μm, respectively. Right: *M. magneticum* strain AMB-1. Cell of the *M. magneticum* strain has an average diameter and length of 0.4 ± 0.1 and 2.5 ± 0.6 μm, respectively. The averages are calculated from 15 TEM images for each bacterial strain, and depend on the growth conditions. The morphology of each bacterial strain determined by these TEM images is used in (6) to calculate the rotational drag coefficients and the magnetic dipole moments.

Manuscript received April 22, 2013; revised August 15, 2013; accepted October 9, 2013. Date of publication October 28, 2013; date of current version April 4, 2014. Corresponding author: I. S. M. Khalil (e-mail: islam.shoukry@guc.edu.eg) and S. Misra (e-mail: s.misra@utwente.nl).

Color versions of one or more of the figures in this paper are available online at http://ieeexplore.ieee.org.

Digital Object Identifier 10.1109/TMAG.2013.2287495

magnetite nanocrystals that are enveloped in the cell of the MTB, as shown in Fig. 1. A magnetospectrophotometry assay was used to characterize the bacterial magnetism and analyze the alignment of the magnetotactic bacteria (*M. magneticum* strain AMB-1) in magnetic fields [16]. This technique is based on the application of magnetic fields and measuring the corresponding change in the light scattering when the bacteria swim across the light beam. Komeili *et al.* [4] characterized the cell biology of the magnetosome of the magnetotactic bacteria (*M. magneticum* strain AMB-1) and showed that magnetosome vesicles can exist before magnetite biomineralization. Characterization of the magnetic dipole moment is necessary for the realization of the closed-loop control of an MTB, since the characterized magnetic dipole moment is used in the magnetic force– and magnetic torque–current maps. These maps are used in the realization of the closed-loop controllers for magnetic-based manipulation systems [17], [23], [24].

Lu and Martel [25], [26] demonstrated the open-loop control of a swarm of Magnetococcus marinus strain MC-1 inside microchannels of 50–120 μm in diameter. It was further shown that a swarm of flagellated magnetotactic bacteria can be used to accurately manipulate microcomponents via the thrust force generated by the flagella bundles [27]. Motile bacteria (Serratia marcescens strain Db11) were integrated with a microstructure and controlled by the self-propulsion and dc electric fields using a vision feedback control system [10]. Closed-loop control of an MTB, i.e., *M. magnetotacticum* strain MS-1, was accomplished by characterizing its magnetic dipole moment and realizing a proportional-derivative control system [15]. This control system allowed for the positioning of the MTB within the vicinity of the reference position.

In this paper, we analyze the closed-loop control characteristics of two species of magnetotactic bacteria that are grown according to the recommended conditions [30]. This analysis is done by comparing the control characteristics of cells of *M. magnetotacticum* and *Magnetospirillum magneticum*, in the transient and steady states. The transient state is evaluated by the average velocity of the controlled cells, whereas the steady state is evaluated by the average diameter of the region of convergence in which the cell is positioned by the closed-loop control inputs. First, the magnetic dipole moments of these two strains are characterized using the U-turn technique, the rotating-field technique, and the flip-time technique. The characterized average magnetic dipole moment is then used in the realization of closed-loop control systems for each bacterial strain. Each closed-loop control system is based on the magnetic force–current map of each bacterial strain. The characterized magnetic properties in this paper depend on the growth conditions of the two bacterial strains and different properties can be achieved. Therefore, we follow the recommended growth conditions of each strain to perform our comparative study. This comparative study could allow us to choose certain bacterial strain as a biological microrobot based on its closed-loop control characteristics.

The remainder of this paper is organized as follows. Section II provides the theoretical background pertaining to the modeling of the magnetic force and torque, and the drag force and torque of an MTB. Characterization of the morphology of the *M. magnetotacticum* strain MS-1 and *M. magneticum* strain AMB-1 is done using the transmission electron microscopy (TEM) and the scanning electron microscopy (SEM) images. In addition, the magnetic dipole moments of the strains *M. magnetotacticum* and *M. magneticum* are characterized using the U-turn technique, the rotating-field technique, and the flip-time technique. In Section III, closed-loop control systems are designed for our bacterial strains based on the derived magnetic force–current maps and the characterized magnetic dipole moments. Motion control experimental results of each bacterial strain are provided in Section IV, along with descriptions of the magnetic-based manipulation system. Section V provides a discussion pertaining to the control of the *M. magnetotacticum* strain MS-1 inside a microfabricated maze to analyze the channel wall effect on the closed-loop control characteristics. Finally, Section VI concludes and provides directions for future work.

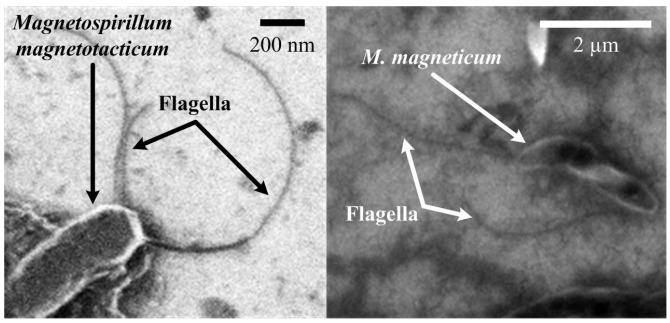

Fig. 2. SEM images of the MTB. The SEM images show the flagella of the MTB. An MTB moves along the magnetic field lines using its flagella. Left: *M. magnetotacticum* strain MS-1. The cell has flagella with average length and thickness of 12 ± 3 μm and $\sim$20 nm, respectively. Right: *M. magneticum* strain AMB-1. The cell has flagella with average length and thickness of 7 ± 2 μm and $\sim$20 nm, respectively. The averages are calculated from 15 SEM images for each bacterial strain, and depend on the recommended growth conditions. The morphology of each bacterial strain determined by these SEM images is used in (6) to calculate the rotational drag coefficients and the magnetic dipole moments. The SEM images are analyzed using ImageJ 1.45 s (ImageJ, Image Processing and Analysis in Java, USA).

II. Modeling and Characterization of Magnetotactic Bacteria

Motion of an MTB in a low Reynolds number regime is governed by the magnetic force and torque exerted on its magnetite nanocrystals, the viscous drag force and torque, and the propulsion force and torque generated by the flagella of the MTB. In this section, we model the motion of an MTB. In addition, the morphologies and magnetic dipole moments of the strains *M. magnetotacticum* and *M. magneticum* are characterized. The magnetic dipole moment of motile magnetotactic bacteria is characterized using the U-turn and rotating-field techniques, whereas the magnetic dipole moment of the nonmotile magnetotactic bacteria is characterized using the flip-time technique.

A. Modeling of Magnetotactic Bacteria

Under the influence of an external magnetic field, the magnetic force ($\mathbf{F}(\mathbf{P}) \in \mathbb{R}^{3\times 1}$) experienced by an MTB located

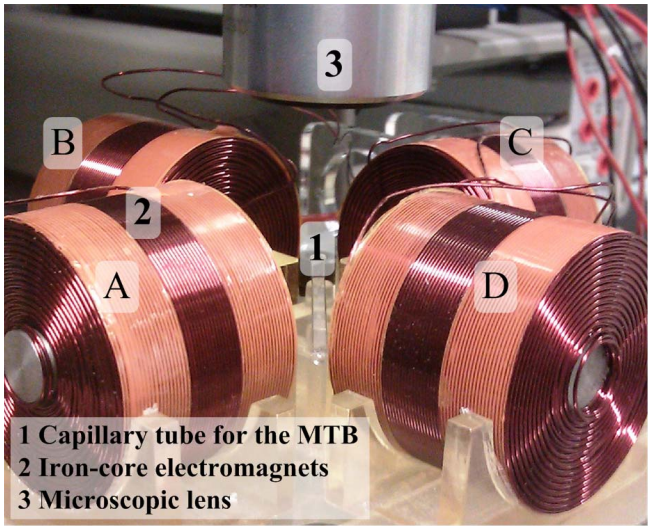

Fig. 3. Magnetic-based manipulation system developed for the characterization and control of magnetotactic bacteria by the magnetic fields generated at each of the electromagnets. The system consists of a microscope equipped with a vision system mounted on the top of an array of electromagnets surrounding a flat capillary tube containing suspensions of cells in growth medium [32]. The capillary tube has an inner thickness, an inner width, and length of 0.2, 2, and 50 mm, respectively (VitroCom, VitroTubes 3520-050, Mountain Lakes, USA). The electromagnets are labeled with the letters A, B, C, and D.

at position ($\mathbf{P} \in \mathbb{R}^{3\times1}$) is given by [8]

$$\mathbf{F}(\mathbf{P}) = (\mathbf{m} \cdot \nabla)\mathbf{B}(\mathbf{P}) \tag{1}$$

where $\mathbf{m} \in \mathbb{R}^{3\times1}$ and $\mathbf{B}(\mathbf{P}) \in \mathbb{R}^{3\times1}$ are the magnetic dipole moment of the MTB and the induced magnetic field, respectively. The magnetic torque ($\mathbf{T}(\mathbf{P}) \in \mathbb{R}^{3\times1}$) exerted on the magnetite nanocrystals of the MTB is given by

$$\mathbf{T}(\mathbf{P}) = \mathbf{m} \times \mathbf{B}(\mathbf{P}). \tag{2}$$

Magnetotactic bacteria passively align along the external magnetic field due to a torque on their magnetic dipole. These magnetic microorganisms move along the field lines using the thrust forces generated by their flagella (Fig. 2). The propulsion force and torque generated by the magnetic fields and the flagella bundles must overcome the viscous drag force and torque, respectively.

An MTB experiences a viscous drag force (F_{d}) given by

$$F_{\mathrm{d}} = \gamma\, \upsilon \tag{3}$$

where υ ($|\dot{\mathbf{P}}| = \upsilon$) is the linear velocity of the MTB. Furthermore, γ is the linear drag coefficient and is given by [28]

$$\gamma = 2\pi\, \eta l \left[\ln\left(\frac{2l}{d}\right) - 0.5\right]^{-1} \tag{4}$$

where η, l, and d are the dynamic viscosity of the medium, length, and diameter of the cell, respectively. The viscous drag torque (T_{d}) is given by

$$T_{\mathrm{d}} = \alpha\omega \tag{5}$$

TABLE I

MORPHOLOGY OF THE *M. Magnetotacticum* AND *M. Magneticum* STRAINS: THE CHARACTERISTICS ARE CALCULATED FROM 15 SEM/TEM IMAGES OF EACH BACTERIAL STRAIN.*

Characteristics	***Magnetospirillum magnetotacticum***	***M. magneticum***
Cell length (l) [μm]	5.2 ± 0.5	2.5 ± 0.6
Cell diameter (d) [μm]	0.5 ± 0.1	0.4 ± 0.1
Flagellum length [μm]	12 ± 3	7 ± 2
Flagellum thickness [nm]	$\sim$20	$\sim$20
Nano-crystals morphology	cuboctahedral	cuboctahedral
Nano-crystals edge length [nm]	30 ± 8	29 ± 13
Number of nano-crystals	18 ± 5	15 ± 7

*These results are used in the characterization of the rotational drag coefficients using (6), and the magnetic dipole moments of the magnetotactic bacteria using (9), (10), and (12). These results are based on the recommended growth condition of the two bacterial strains. The SEM and TEM images are analyzed using ImageJ 1.45 s (ImageJ, Image Processing, and Analysis in Java, USA)

where ω is the angular velocity of the MTB. Further, α is the rotational drag coefficient and is given by [29]

$$\alpha = \frac{\pi\, \eta l^3}{3}\left[\ln\left(\frac{l}{d}\right) + 0.92\left(\frac{d}{l}\right) - 0.662\right]^{-1}. \tag{6}$$

The linear motion of an MTB in a fluid is governed by

$$|\mathbf{F}(\mathbf{P})| + F_{\mathrm{d}} + f = 0 \tag{7}$$

where f is the propulsion force generated by the helical flagella. Furthermore, the rotational motion of an MTB is governed by

$$|\mathbf{T}(\mathbf{P})| + T_{\mathrm{d}} + \boldsymbol{\Omega} = 0 \tag{8}$$

where $\boldsymbol{\Omega}$ is the torque generated by the helical flagella. In this paper, the force equation (7) is used to realize the closed-loop control system of the MTB, whereas the torque equation (8) is used in the computation of the magnetic dipole moment using the rotating-field technique. This computation requires the characterization of the morphology of the MTB.

B. Characterization of Magnetotactic Bacteria

In this paper, the magnetotactic bacterial strains are *M. magnetotacticum* (ATCC 31632) and *M. magneticum* (ATCC 700264). The *M. magnetotacticum* and *M. magneticum* cells are incubated in MSGM mediums (ATCC 1653) with oxygen concentration of approximately 1% [30]. The cultures are incubated at 30 °C for four to 10 days. Cells are harvested when small gray sediments are visible at the bottom of the tubes. The growth conditions of the magnetotactic bacteria affect their characteristics and different magnetic properties can be achieved based on these conditions [2], [35]. Calculation of the magnetic dipole moment (1) and (2) and the linear and rotational drag coefficients (4) and (6) necessitates the determination of the morphology of the MTB. We use SEM and TEM images to determine the morphology of the cells (Table II-A). The morphology is determined from 15 SEM and TEM images of each bacterial strain. These images are analyzed using ImageJ 1.45s (ImageJ, Image Processing, and Analysis in Java, USA).

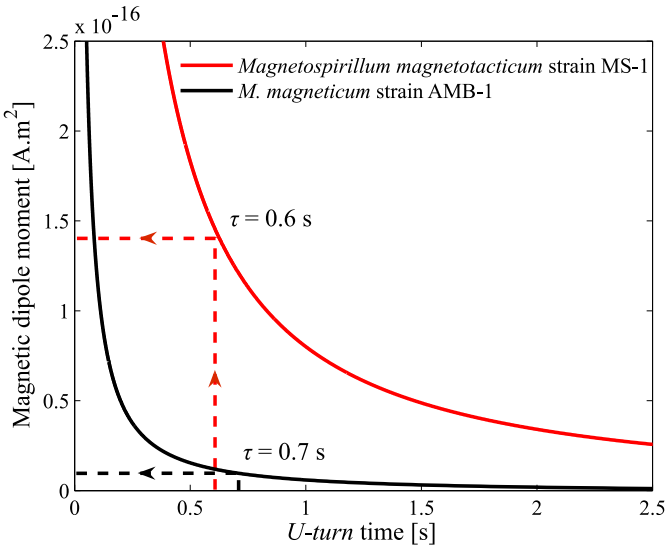

Fig. 4. Relation between the magnetic dipole moment and the U-turn time for the *M. magnetotacticum* and *M. magneticum* strains, using (10). This relation shows that cells with greater magnetic dipole moment have the ability to perform faster U-turn trajectories. The characterized morphologies of these cells are used to realize the relations between the magnetic dipole moment and the U-turn time. Morphology of the *M. magnetotacticum* strain MS-1: $l = 5.2$ μm and $d = 0.5$ μm. Morphology of the *M. magneticum* strain AMB-1: $l = 2.5$ μm and $d = 0.4$ μm. l and d are the length and diameter of the cell, respectively. The magnetic field and the dynamic viscosity of the fluid are 7.9 mT and 1 mPa.s, respectively. The magnetic dipole moment calculated by the U-turn time is used along with the result of the U-turn diameter (9) to determine the average magnetic dipole moment.

1) Magnetic Dipole Moment (U-Turn Technique): The magnetic dipole moment of our motile magnetotactic bacteria is determined using the U-turn technique [11], [31]. An MTB undergoes U-turn trajectories under the reversal of the magnetic fields. The U-turn diameter is given by

$$D = \frac{\alpha \pi \upsilon}{|\mathbf{m}||\mathbf{B}(\mathbf{P})|} \tag{9}$$

where D is the diameter of the U-turn. The U-turn time is

$$\tau = \frac{\alpha}{|\mathbf{m}||\mathbf{B}(\mathbf{P})|} \ln\left(\frac{2\,|\mathbf{m}||\mathbf{B}(\mathbf{P})|}{\mathrm{k}T}\right) \tag{10}$$

where τ is the time of the U-turn. Furthermore, k and T are the Boltzmann's constant and the temperature of the fluid, respectively. Using (9) and (10), we calculate the magnetic dipole moment for each strain of our MTB. Therefore, we determine the diameter and the time of the U-turn trajectory of the MTB. The magnetic-based manipulation system shown in Fig. 3 is used to provide magnetic fields and field reversals. Diameter and time of the U-turn trajectories are determined from the motion of the cells. Our magnetic-based manipulation system consists of an orthogonal array of electromagnets, which surrounds a capillary tube containing suspensions of cells in growth medium [15]. A microscopic vision system is mounted on the top of the array of electromagnets to track the motion of the cells using our feature tracking software [32].

The average U-turn diameter and time are calculated from 10 U-turn trajectories for each bacterial strain. In this experiment, electromagnet A (Fig. 3) is used to generate uniform magnetic fields and field reversals. We calculate the rotational drag coefficient (6) for each strain using the characterized morphology provided in Table II-A. We assume that the growth medium of our magnetotactic bacteria has similar properties as water. Fig. 4 shows the relation between the magnetic dipole moment and the U-turn time for the strains *M. magnetotacticum* and *M. magneticum*. This relation shows that the bacterial strain with greater magnetic dipole moment undergoes U-turn trajectories in shorter time. Cells of *M. magnetotacticum* strain MS-1 have an average U-turn diameter and time of 16 μm and 0.6 s, respectively. Using (9) and (10), the calculated magnetic dipole moments of these cells are 1.8×10^{-16} and 1.4×10^{-16} A.m^2, respectively, at magnetic field of 7.9 mT and average linear velocity of 32 μm/s. Therefore, the average magnetic dipole moment of the cells of *M. magnetotacticum* using the U-turn technique is 1.6×10^{-16} A.m^2 (Table II-B.1). Cells of *M. magneticum* strain AMB-1 have an average U-turn diameter and time of 8.9 μm and 0.7 s, respectively. Using (9) and (10), the calculated magnetic dipole moments of these cells are 1.9×10^{-17} and 1.2×10^{-17} A.m^2, respectively, at magnetic field of 7.9 mT and average linear velocity of 30 μm/s. Therefore, the average magnetic dipole moment of the cells of *M. magneticum* using the U-turn technique is 1.5×10^{-17} A.m^2. The experimental results of the U-turn technique are provided in Fig. 5(a) and (b) for the *M. magnetotacticum* and *M. magneticum* strains, respectively. Table II-B.1 provides the characterized average magnetic dipole moment of each bacterial strain.

TABLE II
CHARACTERIZED MAGNETIC DIPOLE MOMENT OF THE *M. Magnetotacticum* STRAIN MS-1 AND *M. Magneticum* STRAIN AMB-1 USING THE U-TURN, THE ROTATING-FIELD, AND THE FLIP-TIME TECHNIQUES.*

Characteristics	***Magnetospirillum magnetotacticum***	***M. magneticum***
U-turn diameter (D) [μm]	16 ± 3.1	8.9 ± 1.8
U-turn time (τ) [s]	0.6 ± 0.2	0.7 ± 0.3
Dipole moment ($\mid \mathbf{m} \mid$) [A.m^2]	1.6×10^{-16}	1.5×10^{-17}
Boundary frequency (ω_b) [rad/s]	9.5 ± 1.7	8.1 ± 2.6
Dipole moment ($\mid \mathbf{m} \mid$) [A.m^2]	1.3×10^{-16}	1.5×10^{-17}
Flip-time (τ) [s]	1.4 ± 0.7	2.7 ± 0.8
Dipole moment ($\mid \mathbf{m} \mid$) [A.m^2]	0.5×10^{-16}	0.1×10^{-17}

*The averages are calculated from 10 characterization experiments for each bacterial strain. The characterization experiments are done at a magnetic field of 7.9 mT, and linear velocities of 32 and 30 μm/s for the *M. Magnetotacticum* and *M. Magneticum* strains, respectively. Equations (9) and (10) are used in the calculation of the average magnetic dipole moment of the cells using the U-turn technique, whereas (10) and (12) are used in the calculation of the average magnetic dipole moment using the flip-time and the rotating-field techniques, respectively. The flip-time technique is used to characterize nonmotile magnetotactic bacteria.

2) Magnetic Dipole Moment (Rotating-Field Technique): Under the influence of a rotating magnetic field, a motile MTB undergoes circular trajectories. The angular velocity of the cells increases by increasing the frequency of the rotating magnetic fields. The cells undergo circular trajectories up to a frequency, i.e., boundary frequency (ω_b), after which the cell can no longer follow the rotating fields. We assume that the torque ($\mathbf{\Omega}$) generated by the helical flagella can be

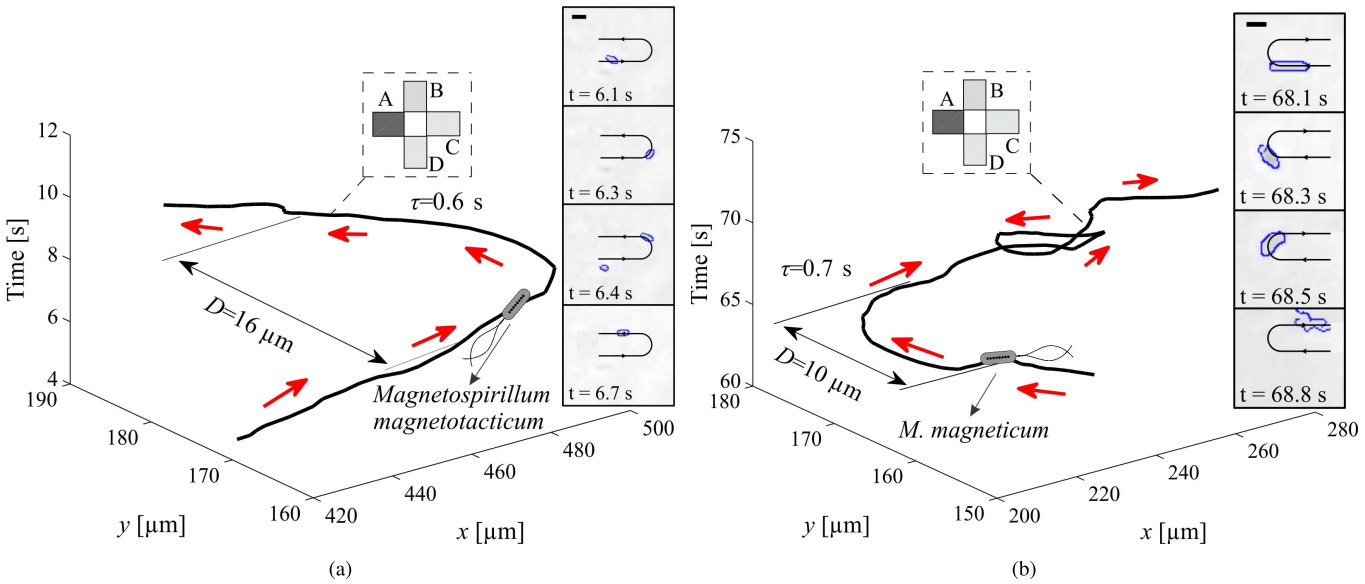

(a) (b)

Fig. 5. Characterization of the magnetic dipole moment of the MTB, i.e., *M. magnetotacticum* strain MS-1 and *M. magneticum* strain AMB-1, using the U-turn technique. Red arrows: the direction of the MTB. Electromagnet A (darker shade) is active during this characterization experiment. The magnetic dipole moment is calculated using (9) and (10), and based on the characterized morphology of the cells. (a) Cell of the *M. magnetotacticum* strain performs a U-turn trajectory, during the magnetic field reversal. The average U-turn diameter is 16 μm. The calculated magnetic dipole moment using (9) is 1.8×10^{-16} A.m^2. The average U-turn time is 0.6 s. The calculated magnetic dipole moment using (10) is 1.4×10^{-16} A.m^2. The average magnetic dipole moment for 10 cells using (9) and (10) is 1.6×10^{-16} A.m^2 at magnetic field of 7.9 mT, and average linear velocity of 32 μm/s. Inset: the U-turn trajectory of an MTB after the reversal of the magnetic field. Black line in the inset: the path of the MTB. The inset images are processed to detect the edges of the cell. Length of the scale bar is 8 μm. (b) Cell of the *M. magneticum* strain performs a U-turn trajectory, during the magnetic field reversal. The average U-turn diameter is 8.9 μm. The calculated magnetic dipole moment using (9) is 1.9×10^{-17} A.m^2. The average U-turn time is 0.7 s. The calculated magnetic dipole moment using (10) is 1.2×10^{-17} A.m^2. The average magnetic dipole moment for 10 magnetotactic bacteria is 1.5×10^{-17} A.m^2 at magnetic field of 7.9 mT, and average linear velocity of 30 μm/s. Inset: the U-turn trajectory of an MTB after the reversal of the magnetic field. Black line in the inset: the path of the MTB. The inset images are processed to detect the edges of the cell. Length of the scale bar is 5 μm.

ignored [12]. Therefore, using (8), the relation between the magnetic torque and the angular velocity of the cell (ω) is given by

$$|\mathbf{m}||\mathbf{B}(\mathbf{P})|\sin\beta + \alpha\omega = 0 \tag{11}$$

where β is the angle between the induced magnetic field and the magnetic dipole moment of the MTB. Characterization of the magnetic dipole moment requires the determination of its boundary frequency (ω_b). This frequency can be determined by gradually increasing the frequency of the rotating field and observing the frequency after which the cell can no longer follow the rotating magnetic fields, i.e., $\omega = \omega_b$, when $\sin\beta = 1$. Therefore, (11) can be written as

$$|\mathbf{m}||\mathbf{B}(\mathbf{P})| + \alpha\omega_b = 0. \tag{12}$$

We use our magnetic-based manipulation system to generate rotating magnetic fields using electromagnets A and D. The frequency of the rotating fields is increased gradually to determine the boundary frequency of each bacterial strain. This experiment is done using 10 cells from each bacterial strain. The average boundary frequency of the cells of *M. magnetotacticum* and *M. magneticum* strains are 9.5 and 8.1 rad/s, respectively. Using (12), the average magnetic dipole moment of the *M. magnetotacticum* and *M. magneticum* cells, at magnetic field of 7.9 mT, are 1.3×10^{-16} and 1.5×10^{-17} A.m^2, respectively. The experimental results of the rotating-field technique are shown in Fig. 6(a) and (b) for the *M. magnetotacticum* and *M. magneticum* strains, respectively. Table II-B.1 provides the characterized average magnetic dipole moment of each bacterial strain.

3) Magnetic Dipole Moment (Flip-Time Technique): During magnetic field reversals, nonmotile magnetotactic bacteria exhibit flip turns. The flip time of each turn can be determined from the motion analysis of the cells. The flip time is given by (10). The top and bottom rows of Fig. 7 show representative experimental results of the characterization of the magnetic dipole moment using the flip-time technique for the *M. magnetotacticum* and *M. magneticum* cells, respectively. Uniform magnetic fields are generated using electromagnet A (Fig. 3). Once the magnetic field is reversed, we start recording the flip time of the cell. The flip time is determined when the cell accomplishes approximately 180° flip turn. We repeat this experiment using 10 different cells for each strain. The average flip time of the *M. magnetotacticum* and *M. magneticum* cells are 1.4 and 2.7 s, respectively. The corresponding average magnetic dipole moments are calculated for each bacterial strain using the characterized morphology (Table II-A) and (10). The calculated average magnetic dipole moments of the *M. magnetotacticum* and *M. magneticum* cells are 0.5×10^{-16} and 0.1×10^{-17}, respectively, at a magnetic field of 7.9 mT. Table II-B.1 provides the characterized average magnetic dipole moments of the motile and nonmotile *M. magnetotacticum* and *M. magneticum* cells. It is important to note that (10) represents the U-turn time and flip time for motile and nonmotile magnetotactic bacteria, respectively.

4) Dipole Moment (TEM): The total volume of the magnetite nanocrystals is deduced from the TEM images of the

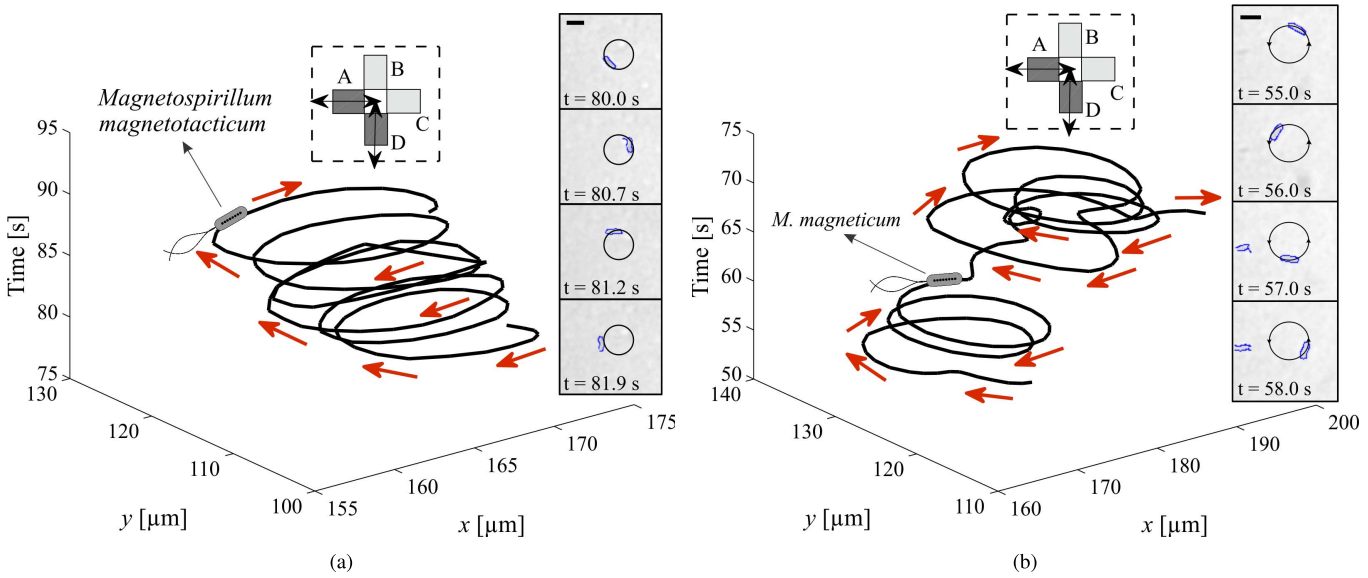

Fig. 6. Characterization of the magnetic dipole moment of the MTB, i.e., *M. magnetotacticum* strain MS-1 and *M. magneticum* strain AMB-1, using the rotating-field technique. Red arrows: the direction of the MTB. Electromagnets A and B (darker shade) are active during this characterization experiment. Magnetic dipole moment is calculated using (12). (a) Cell of the *M. magnetotacticum* strain undergoes circular trajectories under the influence of the rotating fields. The average boundary frequency is 9.5 rad/s. The average magnetic dipole moment is 1.3×10^{-16} A.m^2, at magnetic field of 7.9 mT. Inset: the circular motion of an MTB under the influence of rotating magnetic fields. Black circle in the inset: the circular path of the MTB. The inset images are processed to detect the edges of the cell. Length of the scale bar is 5 μm. (b) Cell of the *M. magneticum* strain undergoes circular trajectories under the influence of the rotating fields. The average boundary frequency is 8.1 rad/s. The average magnetic dipole moment is 1.5×10^{-17} A.m^2, at magnetic field of 7.9 mT. Inset: the circular motion of an MTB under the influence of rotating magnetic fields. Black circle in the inset: the circular path of the MTB. The inset images are processed to detect the edges of the cell. Length of the scale bar is 3 μm.

cells, and used in the calculation of their magnetic dipole moments. The magnetic dipole moment has an upper limit that is given by

$$|\mathbf{m}| = \sigma \sum_{j=1}^{k} m_j \tag{13}$$

where σ is the saturation magnetization of magnetite (60 A.m^2/kg) [34]. Furthermore, k and m_j are the number and volume of the jth magnetite nanocrystal, respectively. Using (13), the upper limits of the magnetic dipole moments are calculated to be 2.9×10^{-16} and 2.1×10^{-16} A.m^2 for the *M. magnetotacticum* and *M. magneticum* cells, respectively. We observe that the average magnetic dipole moments calculated from the TEM images are higher than these obtained from the motion analysis-based techniques. We attribute the difference between these values to the assumption that the nanocrystal chains are perfectly straight and the magnetic dipole moment is the sum of the magnetic moments of each crystal (13). Fig. 1 shows that the nanocrystal chains are curved. Therefore, the effective magnetic dipole moment is less than these values [11]. Our closed-loop control system design is based on the average magnetic dipole moment calculated using the motion analysis-based techniques.

III. Closed-Loop Control System Design

Point-to-point closed-loop control of an MTB is accomplished by controlling the direction of the fields toward a reference position. This control positions the cell within the vicinity of the reference position, but does not achieve zero position tracking error due to the self-propulsion of the cell. We design closed-loop control system based on the magnetic force–current map of each bacterial strain. The magnetic force–current map is used since the magnetic field and the magnetic force lines have the same direction only within the workspace of our magnetic system [36]. Our control system is based on stabilizing the position tracking error of the cell by directing the fields toward the reference position.

A. Magnetic Force–Current Map

We consider a magnetic-based manipulation system with n electromagnets, the magnetic field can be determined by the superposition of the contribution of the ith electromagnet [17]

$$\mathbf{B}(\mathbf{P}) = \sum_{i=1}^{n} \mathbf{B}_i(\mathbf{P}) \tag{14}$$

where $\mathbf{B}_i(\mathbf{P})$ is the induced magnetic field by the ith electromagnet, respectively. Linearity of the magnetic field and the current allows us to rewrite (14) as follows [17]:

$$\mathbf{B}(\mathbf{P}) = \sum_{i=1}^{n} \widetilde{\mathbf{B}}_i(\mathbf{P}) I_i = \widetilde{\mathbf{B}}(\mathbf{P})\mathbf{I} \tag{15}$$

where $\widetilde{\mathbf{B}}(\mathbf{P}) \in \mathbb{R}^{3\times n}$ is a matrix, which depends on the position at which the magnetic field is evaluated, and $\mathbf{I} \in \mathbb{R}^{n\times 1}$ is a vector of the applied current. The magnetic field due to each electromagnet is related to the current input (I_i) by $\widetilde{\mathbf{B}}_i(\mathbf{P})$. Substituting (15) in (1) yields the following magnetic force–current map:

$$\mathbf{F}(\mathbf{P}) = (\mathbf{m}\cdot\nabla)\widetilde{\mathbf{B}}(\mathbf{P})\mathbf{I} = \Lambda(\mathbf{m},\mathbf{P})\mathbf{I} \tag{16}$$

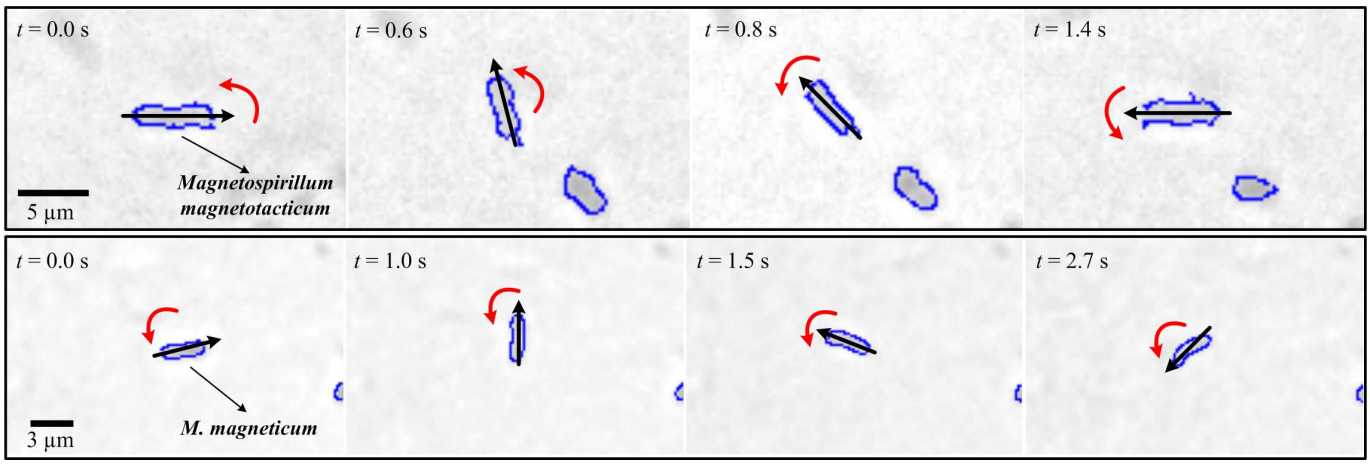

Fig. 7. Characterization of the magnetic dipole moment of nonmotile MTB, i.e., *M. magnetotacticum* strain MS-1 and *M. magneticum* strain AMB-1, using the flip-time technique. An MTB undergoes counter-clockwise flip turn when it is subjected to a magnetic field reversal. The flip time is determined starting from the initiation time of the field reversal until the cell accomplishes approximately 180° turn. Curved red arrow: the direction of rotation of the cell after the reversal of the magnetic field. The average magnetic dipole moment is calculated using (10) from 10 different cells from each strain. Top: cell of the *M. magnetotacticum* strain undergoes a flip turn when the magnetic field is reversed. The average flip time is 1.4 s. The average magnetic dipole moment is 0.5×10^{-16} A.m^2, at magnetic field of 7.9 mT. Bottom: cell of the *M. magneticum* strain undergoes a flip turn when the magnetic field is reversed. The average flip time is 2.7 s. The average magnetic dipole moment is 0.1×10^{-17} A.m^2, at magnetic field of 7.9 mT. These images are processed to detect the edges of the cells.

where $\Lambda(\mathbf{m},\mathbf{P}) \in \mathbb{R}^{3\times n}$ is the actuation matrix, which maps the input current to the magnetic force [17]. The magnetic force–current map (16) depends on the characterized magnetic dipole moment of each bacterial strain. Therefore, we design closed-loop control system based on the force–current map of each bacterial strain [18]. This closed-loop control system must stabilize the position tracking error of the MTB to control its motion. The average magnetic dipole moment of the motile cells is used in the realization of the magnetic force–current map (16).

B. Position Tracking Error Dynamics

We calculate the position and velocity tracking errors of the MTB with respect to a fixed reference position ($\mathbf{P_{ref}}$)

$$\mathbf{e} = \mathbf{P} - \mathbf{P_{ref}}, \quad \dot{\mathbf{e}} = \dot{\mathbf{P}} - \dot{\mathbf{P}}_{\mathbf{ref}} = \dot{\mathbf{P}} \tag{17}$$

where $\mathbf{e}$ and $\dot{\mathbf{e}}$ are the position and velocity tracking errors, respectively. We devise a desired magnetic force ($\mathbf{F_{des}(P)}$) of the form

$$\mathbf{F_{des}(P)} = \mathbf{K_p e} + \mathbf{K_d}\dot{\mathbf{e}}. \tag{18}$$

In (18), $\mathbf{K_p}$ and $\mathbf{K_d}$ are the controller positive-definite gain matrices, and are given by

$$\mathbf{K_p} = \begin{bmatrix} k_{\mathrm{p1}} & 0 \\ 0 & k_{\mathrm{p2}} \end{bmatrix}, \quad \mathbf{K_d} = \begin{bmatrix} k_{\mathrm{d1}} & 0 \\ 0 & k_{\mathrm{d2}} \end{bmatrix} \tag{19}$$

where $k_{\mathrm{p}r}$ and $k_{\mathrm{d}r}$, for $(r = 1, 2)$, are the proportional and derivative gains, respectively. Substituting (18) in the magnetic force equation (7), i.e., $\mathbf{F_{des}(P)} = \mathbf{F(P)}$, and assuming no propulsion force ($f = 0$) yields the following position tracking error dynamics:

$$\dot{\mathbf{e}} + (\mathbf{K_d} + \gamma\,\Pi)^{-1}\,\mathbf{K_p e} = 0 \tag{20}$$

where Π is the identity matrix. Since $f \neq 0$, zero position tracking error cannot be achieved. However, the closed-loop control system positions the cell within the vicinity of the reference position, i.e., a region of convergence, based on (20). Therefore, the positioning accuracy of the closed-loop control system depends on the dynamic viscosity of the growth medium, morphology of the cells, the propulsion force of the flagella, and the controller gains. We evaluate the accuracy of the closed-loop control system using the size of the region of convergence.

IV. Experimental Results

The magnetic-based manipulation system (Fig. 3) is used during the closed-loop control of the *M. magnetotacticum* and *M. magneticum* cells. In this experiment, multiple reference positions are given to the control system (18) to examine the point-to-point positioning of the controlled cells. Fig. 8 shows a representative motion control trial of *M. magnetotacticum* cell. The closed-loop control system allows for the positioning of the cell at an average velocity of 24 μm/s, and within the vicinity of three reference positions. The region of convergence has diameters of 28, 10, and 11 μm. For the same controller gains, the closed-loop control system (based on the characterized magnetic dipole moment of the *M. magneticum* strain) positions the cell at an average velocity of 22 μm/s. The control system positions the cell within the vicinity of three reference positions with region of convergence of 26, 12, and 29 μm in diameter, as shown in Fig. 9. We calculate the average velocity and region of convergence from 10 different closed-loop control trials at the same controller gains. Table IV provides a comparison between the control characteristics of the *M. magnetotacticum* and *M. magneticum* cells at the transient and steady states. The transient state is represented by the average velocity of the controlled cells, whereas the steady state is represented by the average diameter of the region of convergence. We observe that cells of *M. magnetotacticum* strain are controlled at an average velocity of 32 ± 10 μm/s (approximately seven body lengths per second), whereas

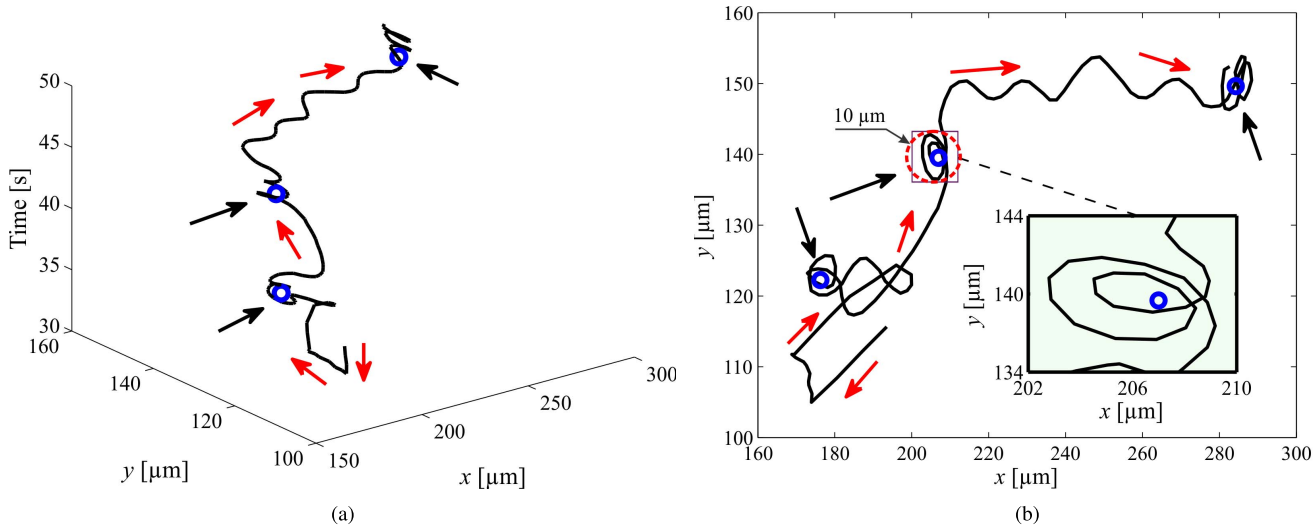

Fig. 8. Closed-loop control of the strain *M. magnetotacticum* inside a capillary tube (VitroCom, VitroTubes 3520-050, Mountain Lakes, USA) with inner width and thickness of 1 and 0.2 mm, respectively. The MTB is controlled using the control law (18). The controller gains are $k_{p1} = k_{p2} = 15.0\ s^{-2}$ and $k_{d1} = k_{d2} = 15.5\ s^{-1}$. Red arrows: the direction the controlled MTB. Blue circles: the reference positions (shown by the black arrows). (a) MTB follows three reference positions at an average velocity of 24 μm/s. (b) Closed-loop control system positions an MTB within the vicinity of the reference positions. Inset: MTB is positioned within a region of convergence of 10 μm in diameter (red dashed circle). The diameters of the region of convergence of the three reference positions are 28, 10, and 11 μm.

cells of *M. magneticum* strain are controlled at an average velocity of 30 ± 12 μm/s (approximately eight body lengths per second). Furthermore, the control system positions the aforementioned bacterial strains within an average region of convergence of 23 ± 10 and 35 ± 14 μm, respectively.

Our closed-loop motion control results show that the response (average velocity) of cells of the *M. magnetotacticum* strain is 6.2% greater than the response of cells of the *M. magneticum* strain. In addition, the positioning accuracy (diameter of the region of convergence) of the *M. magnetotacticum* cells is 7% greater than the *M. magneticum* cells, for the same controller gains. This accuracy allows our closed-loop control system to position an MTB within a smaller region of convergence. The motion analysis-based characterization results show that the magnetic dipole moment of the *M. magnetotacticum* strain is one order of magnitude greater than the magnetic dipole moment of the *M. magneticum* strain. Fig. 4 shows that the magnetic dipole moment exponentially decreases with respect to the U-turn time. Therefore, the best hypothesis for the greater positioning accuracy of the *M. magnetotacticum* cells is the magnitude of the magnetic dipole moment. This magnetic dipole moment allows the controlled cells to perform faster U-turns, i.e., shorter U-turn time, during the magnetic field reversals. This would allow the cell to be positioned within a smaller region of convergence, as opposed to a cell with a smaller magnetic dipole moment. The closed-loop control system reverses the magnetic fields when a controlled cell reaches a reference position to reduce the position tracking error, based on (20). The bacterial strain with a greater magnetic dipole moment undergoes faster U-turn trajectories. Therefore, this response would allow the *M. magnetotacticum* cells to be positioned within a smaller region of convergence, as opposed the *M. magneticum* cells.

TABLE III

CLOSED-LOOP CONTROL RESULTS OF THE STRAINS *M. Magnetotacticum* AND *M. Magneticum*. TRANSIENT-STATE IS EVALUATED BY THE AVERAGE VELOCITY OF THE CONTROLLED MTB, WHEREAS STEADY STATE IS EVALUATED BY THE AVERAGE DIAMETER OF THE REGION OF CONVERGENCE.*

Characteristics	***Magnetospirillum magnetotacticum***	***M. magneticum***
Velocity [μm/s]	32 ± 10	30 ± 12
Region-of-convergence [μm]	23 ± 10	35 ± 14

*The average is calculated from 10 closed-loop motion control trials with the same controller gains using (18). The controller gains are $k_{p1} = k_{p2} = 15.0\ s^{-2}$ and $k_{d1} = k_{d2} = 15.5\ s^{-1}$.

V. DISCUSSION

Our comparative study between the *M. magnetotacticum* and *M. magneticum* strains shows that the *M. magnetotacticum* cells have slightly greater tendency to provide desirable closed-loop control characteristics. These characteristics include the average velocity and positioning accuracy. The methods and results of this comparative study can be used in the selection of a bacterial strain as a biological microrobot during the execution of nontrivial tasks such as microactuation, micromanipulation, microassembly, and targeted drug delivery. The first three tasks require characterization of the self-propulsion force of each bacterial strain. Furthermore, the targeted drug delivery task requires the investigation of the closed-loop behavior of the bacterial strains under the influence of channel wall effect and flowing fluid streams. In [37], the channel wall effect was experimentally investigated. We developed a microfabricated maze with channel width of 10 μm. This maze was mounted in the center of the array

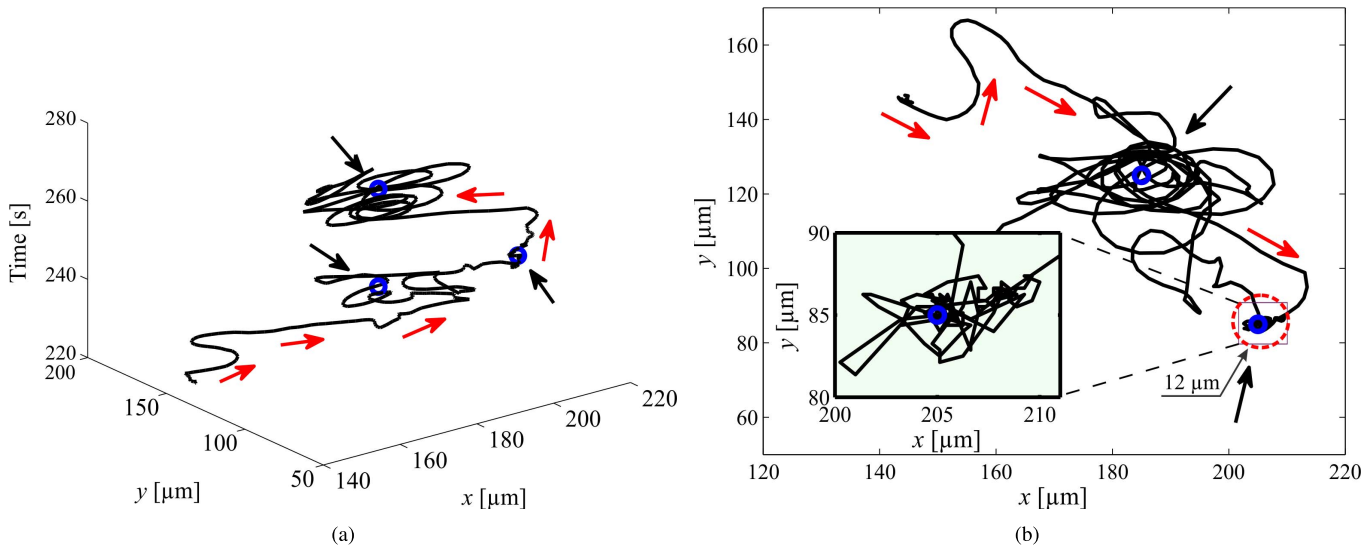

Fig. 9. Closed-loop control of the strain *M. magneticum* inside a capillary tube (VitroCom, VitroTubes 3520-050, Mountain Lakes, USA) with inner width and thickness of 1 and 0.2 mm, respectively. The MTB is controlled using the control law (18). The controller gains are $k_{p1} = k_{p2} = 15.0\ s^{-2}$ and $k_{d1} = k_{d2} = 15.5\ s^{-1}$. Red arrows: the direction of the controlled MTB. Blue circles: the reference positions (shown by the black arrows). (a) MTB follows three reference positions at an average velocity of 22 μm/s. (b) Closed-loop control system positions an MTB within the vicinity of the reference positions. Inset: MTB is positioned within a region of convergence of 12 μm in diameter (red dashed circle). The diameters of the region of convergence of the three reference positions are 26, 12, and 29 μm.

of electromagnets of our magnetic system. Motion control of the cells (*M. magnetotacticum* strain MS-1) was accomplished inside the maze. In this experiment, we observed that the cells move toward the reference positions at an average velocity of 8 μm, and were positioned within a region of convergence of 10 μm. We observe that the average velocity and region of convergence of the controlled cells are decreased by 75% and 56% inside the maze, respectively. We attribute the differences in the average velocity and region of convergence to the channel wall effect of the maze.

All our characterization and closed-loop control experiments are done at the center of flat capillary tubes containing suspensions of cells in growth medium. The velocity of these cells depends on their growth conditions and the oxygen concentration of the medium. Fig. 10(a) shows range of velocities of the cells that we used in this paper. Our closed-loop control system only allows the cells to orient toward the given reference position, then the cell performs a flagellated swim toward the reference position. Once the cell reaches the reference position, the closed-loop control system reverses the direction of the magnetic fields to decrease the position tracking error based on (20). Therefore, the positioning accuracy of the cell depends on the ability of each bacterial strain to perform faster U-turns within the vicinity of a reference position. Using the transient- and steady-state closed-loop characteristics of the controlled bacterial strains (Table IV), we determine the distributions of the velocity and region of convergence, as shown in Fig. 10(a) and (b), respectively. These distributions show that the chance of obtaining similar control results using the *M. magnetotacticum* and *M. magneticum* strains in the transient and steady states are 89% and 40%, respectively. The results provided in this paper are based on the recommended growth conditions of each bacterial strain. Different magnetic and motility properties can be achieved, for instance, by controlling the oxygen concentration in the growth medium [2], [34].

VI. Conclusion

We provide a comparison between the *M. magnetotacticum* strain MS-1 and *M. magneticum* strain AMB-1 by characterizing their morphologies, magnetic dipole moments, and closed-loop control characteristics. This characterization and control comparison is done using a magnetic-based manipulation system. Not only do we find that cells of *M. magnetotacticum* strain have a 6.2% faster response than cells of *M. magneticum* strain, but we also observe that the *M. magnetotacticum* cells have a 7% greater positioning accuracy than the *M. magneticum* cells. However, the chances of obtaining similar response and positioning accuracy are 89% and 40% for the two bacterial strains, respectively. The comparison between the mentioned bacterial strains is done by controlling the motion of their cells using a closed-loop control system. We observe that the cells with greater magnetic dipole moment have a slightly greater tendency to provide desirable steady-state closed-loop control characteristics. This response is due to the relation between the magnetic dipole moment and the time of the U-turn trajectories taken by the cell, as the closed-loop control system reverses the magnetic fields when the cell is positioned within the vicinity of the reference position to decrease the position tracking error. Therefore, cells with greater magnetic dipole moment undergo U-turn trajectories within the vicinity of the reference position in shorter time, and hence providing relatively greater positioning accuracy. The results provided in this paper are based on the recommended growth conditions of each bacterial strain and different magnetic properties can be achieved.

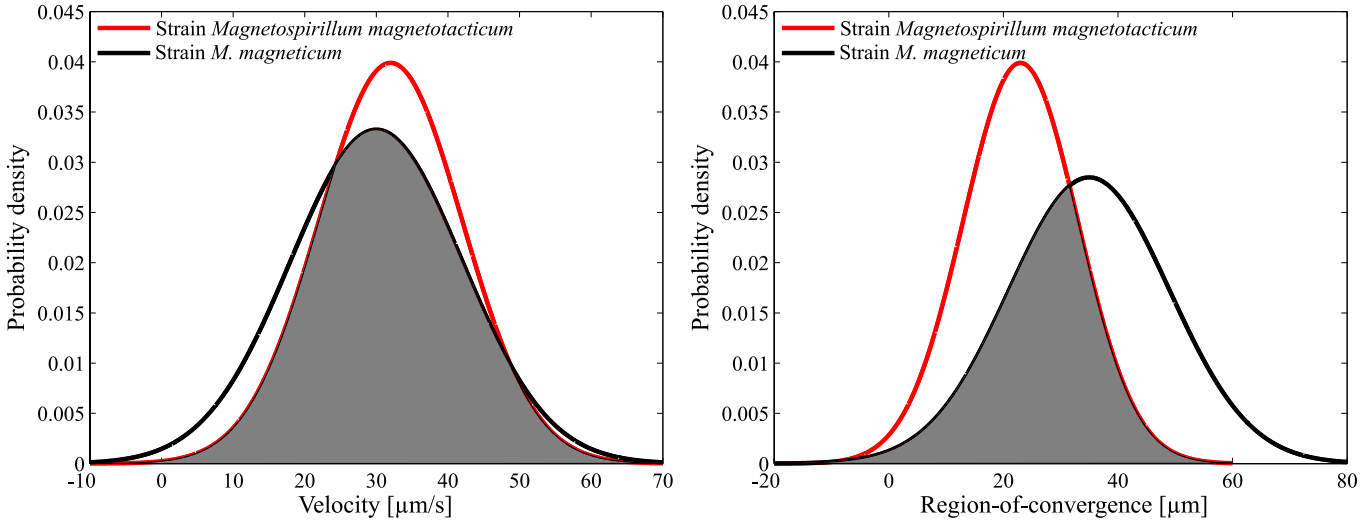

Fig. 10. Distributions of the velocity and region of convergence of the strains *M. magnetotacticum* and *M. magneticum*. The averages and standard deviations used in these results are calculated from 10 closed-loop motion control trials for each bacterial strain. (a) Overlap between these velocity distributions shows that the chance of obtaining similar transient-state characteristics is 89%, for the aforementioned bacterial strains. The average velocities of the controlled strains *M. magnetotacticum* and *M. magneticum* are 32 and 30 μm/s, respectively. (b) Overlap (dark shade) between these two distributions shows that the chance of obtaining similar positioning accuracy is 40%, for the aforementioned bacterial strains. The regions of convergence of the controlled strains *M. magnetotacticum* and *M. magneticum* are 23 and 35 μm in diameter, respectively.

Future work in the field of closed-loop control of magnetotactic bacteria should include a wider comparison between the different bacterial strains, such as the *M. marinus* strain MC-1, *Magnetospirillum gryphiswaldense* strain MSR-1, *M. gryphiswaldense* strain R11, and *M. gryphiswaldense* strain S1. In addition, characterization and control of the MTB in 3-D space will be studied. Our magnetic-based manipulation system will be redesigned to allow for the visual tracking, autofocusing, and control of the MTB in 3-D space. *In vivo* experiments are essential to study the effect of the fluidic flow rates and the time-varying fluid viscosity. Furthermore, closed-loop control of a swarm of magnetotactic bacteria will be studied.

ACKNOWLEDGMENT

This work was supported by the MIRA-Institute for Biomedical Technology and Technical Medicine, University of Twente, The Netherlands. The authors would like to thank M. M. S. M. Wösten, University of Utrecht, Utrecht, The Netherlands, and E. Hadavi, University of Twente, Enschede, The Netherlands, for their valuable feedback during preparation of this paper. They also thank the anonymous reviewers for their valuable feedback and suggestions that improved this paper.

REFERENCES

[1] R. B. Frankel, D. A. Bazylinski, M. S. Johnson, and B. L. Taylor, "Magneto-aerotaxis in marine coccoid bacteria," *Biophys. J.*, vol. 73, no. 2, pp. 994–1000, Aug. 1997.

[2] R. P. Blakemore, R. A. Short, D. A. Bazylinski, C. Rosenblatt, and R. B. Frankel, "Microaerobic conditions are required for magnetite formation within aquaspirillum magnetotacticum," *Geomicrobiol. J.*, vol. 4, no. 1, pp. 53–71, Jan. 1985.

[3] D. Faivre and D. Schuler, "Magnetotactic bacteria and magnetosomes," *Chem. Rev.*, vol. 108, no. 11, pp. 4875–4898, Oct. 2008.

[4] A. Komeili, H. Vali, T. J. Beveridge, and D. K. Newman, "Magnetosome vesicles are present before magnetite formation, and MamA is required for their activation," in *Proc. Nat. Acad. Sci. USA*, vol. 101, no. 11, pp. 3839–3844, Mar. 2004.

[5] H. C. Berg, "Torque generation by the flagellar rotary motor," *Biophys. J.*, vol. 68, pp. 163–167, Apr. 1995.

[6] A. S. Bahaj, P. A. B. James, D. C. Ellwood, and J. H. P. Watson, "Characterization and growth of magnetotactic bacteria: Implcations of clean up of environmental pollusion," *J. Appl. Phys.*, vol. 73, no. 10, pp. 5394–5396, May 1993.

[7] D. A. Bazylinski and R. B. Frankel, "Magnetosomes formation in prokaryotes," *Nature Rev. Microbiol.*, vol. 2, pp. 217–230, Mar. 2004.

[8] S. Martel, O. Felfoul, J.-B. Mathieu, A. Chanu, S. Tamaz, M. Mohammadi, *et al.*, "MRI-based medical nanorobotic platform for the control of magnetic nanoparticles and flagellated bacteria for target interventions in human capillaries," *Int. J. Robot. Res.*, vol. 28, no. 9, pp. 1169–1182, Sep. 2009.

[9] S. Martel, C. C. Tremblay, S. Ngakeng, and G. Langlois, "Controlled manipulation and actuation of micro-objects with magnetotactic bacteria," *Appl. Phys. Lett.*, vol. 89, no. 23, pp. 1–3, 2006.

[10] M. S. Sakar, E. B. Steager, D. H. Kim, A. A. Julius, M. Kim, V. Kumar, *et al.*, "Modeling, control and experimental characterization of microbiorobots," *Int. J. Robot. Res.*, vol. 30, no. 6, pp. 647–658, May 2011.

[11] A. S. Bahaj and P. A. B. James, "Characterisation of magnetotactic bacteria using image processing techniques," *IEEE Trans. Magn.*, vol. 29, no. 6, pp. 3358–3360, Nov. 1993.

[12] K. Erglis, Q. Wen, V. Ose, A. Zeltins, A. Sharipo, P. A. Janmey, *et al.*, "Dynamics of magnetotactic bacteria in a rotating magnetic field," *Biophys. J.*, vol. 93, no. 4, pp. 1402–1412, Aug. 2007.

[13] B. Steinberger, N. Petersen, H. Petermann, and D. G. Wiess, "Movement of magnetic bacteria in time-varying magnetic fields," *J. Fluid Mech.*, vol. 273, pp. 189–211, May 1994.

[14] A. S. Bahaj, P. A. B. James, and F. D. Moeschler, "An alternative method for the estimation of the magnetic moment of non-spherical magnetotactic bacteria," *IEEE Trans. Magn.*, vol. 32, no. 5, pp. 5133–5135, Sep. 1996.

[15] I. S. M. Khalil, M. P. Pichel, L. Zondervan, L. Abelmann, and S. Misra, "Characterization and control of biological microrobots," in *Proc. 13th Int. Symp. Experim. Robot.*, vol. 88. 2013, pp. 617–631.

[16] C. T. Lefevre, T. Song, J.-P. Yonnet, and L.-F. Wu, "Characterization of bacterial magnetotactic behaviors by using a magnetospectrophotometry assay," *Appl. Environ. Microbiol.*, vol. 75, no. 12, pp. 3835–3841, Jun. 2009.

[17] M. P. Kummer, J. J. Abbott, B. E. Kartochvil, R. Borer, A. Sengul, and B. J. Nelson, "OctoMag: An electromagnetic system for 5-DOF wireless micromanipulation," *IEEE Trans. Robot.*, vol. 26, no. 6, pp. 1006–1017, Dec. 2010.

[18] I. S. M. Khalil, M. P. Pichel, L. Abelmann, and S. Misra, "Closed-loop control of magnetotactic bacteria," *Int. J. Robot. Res.*, vol. 32, no. 6, pp. 636–648, May 2013.

[19] S. Floyd, C. Pawashe, and M. Sitti, "Two-dimensional contact and noncontact micromanipulation in liquid using an untethered mobile magnetic microrobot," *IEEE Trans. Robot.*, vol. 25, no. 6, pp. 1332–1342, Dec. 2009.

[20] C. Pawashe, S. Floyd, E. Diller, and M. Sitti, "Two-dimensional autonomous microparticle manipulation strategies for magnetic microrobots in fluidic environments," *IEEE Trans. Robot.*, vol. 28, no. 2, pp. 467–477, Apr. 2012.

[21] P. Valdastri, E. Sinibaldi, S. Caccavaro, G. Tortora, A. Menciassi, and P. Dario, "A novel magnetic actuation system for miniature swimming robots," *IEEE Trans. Robot.*, vol. 27, no. 4, pp. 769–779, Aug. 2011.

[22] B. J. Nelson, I. K. Kaliakatsos, and J. J. Abbott, "Microrobots for minimally invasive medicine," *Annu. Rev. Biomed. Eng.*, vol. 12, pp. 55–85, Apr. 2010.

[23] B. E. Kratochvil, M. P. Kummer, S. Erni, R. Borer, D. R. Frutiger, S. Schüurle, *et al.*, "MiniMag: A hemispherical electromagnetic system for 5-DOF wireless micromanipulation," in *Proc. ISER* (Springer Tracts in Advanced Robotics), vol. 79. 2010, pp. 317–329.

[24] I. S. M. Khalil, V. Magdanz, S. Sanchez, O. G. Schmidt, L. Abelmann, and S. Misra, "Magnetic control of potential microrobotic drug delivery systems: Nanoparticles, magnetotactic bacteria and self-propelled microjets," in *Proc. Int. Conf. IEEE EMBC*, Osaka, Japan, Jul. 2013, pp. 5299–5302.

[25] Z. Lu and S. Martel, "Controlled bio-carriers based on magnetotactic bacteria," in *Proc. IEEE Int. Conf. Solid-State Sensors, Actuat. Microsyst.*, Lyon, France, Jun. 2007, pp. 683–686.

[26] Z. Lu and S. Martel, "Preliminary investigation of bio-carriers using magnetotactic bacteria," in *Proc. 28th Annu. Int. Conf. IEEE EMBS*, New York, NY, USA, Sep. 2006, pp. 683–686.

[27] S. Martel and M. Mohammadi, "Using a swarm of self-propelled natural microrobots in the form of flagellated bacteria to perform complex micro-assembly tasks," in *Proc. IEEE ICRA*, May 2010, pp. 500–505.

[28] H. C. Berg, *Random Walks in Biology*. Princeton, NJ, USA: Princeton Univ. Press, 1993.

[29] Y. R. Chemla, H. L. Grossman, T. S. Lee, J. Clarke, M. Adamkiewicz, and B. B. Buchanan, "A new study of bacterial motion: Superconducting quantum interference device microscopy of magnetotactic bacteria," *Biophys. J.*, vol. 76, pp. 3323–3330, Jun. 1999.

[30] L. E. Bertani, J. Weko, K. V. Phillips, R. F. Gray, and J. L. Kirschvink, "Physical and genetic characterization of the genome of Magnetospirillum magnetotacticum, strain MS-1," *Int. J. Genes Genomes*, vol. 264, pp. 257–263, Jan. 2001.

[31] D. M. S. Esquivel and H. G. P. Lins de Barros, "Motion of magnetotactic microorganisms," *J. Experim. Biol.*, vol. 121, pp. 153–163, Sep. 1986.

[32] J. D. Keuning, J. de Vries, L. Abelmann, and S. Misra, "Image-based magnetic control of paramagnetic microparticles in water," in *Proc. IEEE/RSJ IROS*, San Francisco, CA, USA, Sep. 2011, pp. 421–426.

[33] I. S. M. Khalil, J. D. Keuning, L. Abelmann, and S. Misra, "Wireless magnetic-based control of paramagnetic microparticles," in *Proc. IEEE RAS/EMBS Int. Conf. Biomed. Robot. Biomech.*, Rome, Italy, Jun. 2012, pp. 460–466.

[34] R. L. Reobdos and P. J. Vikesland, "Effects of oxidation on the magnetization of nanoparticulate magnetite," *Amer. Chem. Soc.*, vol. 26, no. 22, pp. 16745–16753, Sep. 2010.

[35] C. T. Lefevre, T. Song, J.-P. Yonnet, and L.-F. Wu, "Characterization of bacterial magnetotactic behaviors by using a magnetospectrophotometry assay," *Appl. Environ. Microbiol.*, vol. 75, no. 12, pp. 3835–3841, Jun. 2009.

[36] J. J. Abbott, O. Ergeneman, M. P. Kummer, A. M. Hirt, and B. J. Nelson, "Modeling magnetic torque and force for controlled manipulation of soft-magnetic bodies," *IEEE Trans. Robot. Autom.*, vol. 23, no. 6, pp. 1247–1252, Dec. 2007.

[37] I. S. M. Khalil, M. P. Pichel, O. S. Sukas, L. Abelmann, and S. Misra, "Control of magnetotactic bacterium in a micro-fabricated maze," in *Proc. IEEE ICRA*, Karlsruhe, Germany, May 2013, pp. 5488–5493.